Journal of Physics: Conference Series **2647** (2024) 052001 doi:10.1088/1742-6596/2647/5/052001

Hydroelastic analysis of flapping-foil thrusters using a partitioned BEM-FEM

D Anevlavi*, E Filippas[1], A Karperaki[2] and K Belibassakis

School of Naval Architecture and Marine Engineering, NTUA, Athens, Greece
*Corresponding author: danevlavi@mail.ntua.gr

Abstract. Understanding the mechanics of aquatic locomotion has been an active field of research for decades and continues to inspire technological solutions ranging from small-scale propulsion systems for autonomous underwater vehicles (AUVs) to larger-scale energy saving devices (ESDs) for ships. The bio-inspired thrust-producing kinematics are shared among most flapping-foil systems, however joint experimental and numerical research suggests that incorporating additional biomimetic features, such as hydrodynamic shape and elasticity, in new designs can enhance the efficiency. Focusing on the latter, the response of passively deforming wings is implicitly non-linear, since deformations affect the hydrodynamic load excitation and vice-versa. Therefore, fluid-structure interaction simulations are essential for accurate predictions of the wings' response. In the present work, a cost-effective computational tool is proposed for the hydroelastic analysis of flexible flapping-foil thrusters, which consists of a 3-D unsteady boundary element method (BEM) weakly coupled with a finite element solver (FEM) based on plate elements. The verification of the present method is accomplished by means of comparison against experimental data from the literature. The prediction capabilities and the limitations of the weakly coupled BEM-FEM are discussed. Finally, the proposed numerical tools serve as the building blocks for the fully coupled BEM-FEM scheme that is currently under development.

1. Introduction

In the past years, numerous flapping-foil applications have sprung from the studies of aquatic swimmers with emphasis on the most efficient locomotion mode evolved in the aquatic environment; the *thunniform* mode found among a group of vertebrates, i.e. sharks, and marine mammals [1]. This swimming mode is characterized by a relatively stiff caudal fin that performs a combination of pitch and heave motions, tracing an oscillating path characterized by a peak-to-peak amplitude, a foil-beat frequency, and a wavelength [2] as shown schematically in Figure 1.The thrust-producing flapping-foil kinematics for non-deforming geometries have been extensively studied both experimentally and numerically with a wide variety of applications [3]. They include small-scale propulsion solutions that resemble fishtails or flukes for autonomous underwater vehicles such as MIT RoboTuna [4] and even larger-scale thrusters operating as auxiliary ship propulsion systems and energy-saving devices (ESDs); see, e.g., the symbiotic ship/engine and propulsion innovation from the SeaTech Horizon 2020 project entitled "Next generation short-sea ship dual-fuel engine and propulsion retrofit technologies"

[1] Department of Naval Architecture, UNIWA, Athens, Greece (current address)
[2] Department of Civil Engineering, Aston University, Birmingham, UK (current address)

(https://seatech2020.eu/), that captures wave energy and reduces ship motions. Particularly, the dynamic wing positioned at the bow operates in a semi-activated regime in terms of pitching motion and is stiffened enough to sustain the hydrodynamic loads [5], [6].

However, fins found in nature are intrinsically elastic and change shape both actively and passively to provide aquatic swimmers with their fascinating abilities. Their autonomous operation comes with exceptional perception of the environment and advanced control [7]. Focusing on the passive deformation of wings and their propulsive performance, experimental research suggests that optimally tuned geometric, kinematic and structural parameters have the potential to enhance efficiency [8], [9]. In any case, replicating a combination of biomimetic features for engineering applications is challenging, requires interdisciplinary insight into the mechanics of fish locomotion and the development of cost-effective computational hydro-elasticity frameworks for research and design [10]. Compliant mechanisms [11] and tailor-made composite wings [12] have been proposed for particular applications; illustrating that manufacturing passively deforming wings that attain maximum efficiency under the design loads is possible.

From a numerical perspective, the response of flexible fins is implicitly nonlinear as deformations affect the hydrodynamic load excitation and vice-versa. Thus, fluid-structure interaction (FSI) coupling is essential for accurate predictions of the wing's response; see, e.g. [13], [14]. Particularly, for the design and analysis of passively deforming thrusters, cost-effective FSI computational tools become valuable especially when they enable fast parametric investigations and hydro-structural optimization studies.

In the present work, we propose a cost-effective computational tool for the hydroelastic analysis of passively deforming flapping-foil thrusters, which consists of a 3-D unsteady boundary element method (BEM) weakly coupled with a finite element solver (FEM) based on discrete Kirchhoff plate elements (DKT). The verification of the present method is accomplished by means of comparisons against experimental data from the literature. The developed computational tool, based on the weakly coupled version, is found to predict the amplitude of wing deformation with acceptable accuracy. Certain trends for the effects of motion frequency and material properties on the average thrust coefficient and propulsive efficiency are also in agreement with the experimental data. However, the weak coupling approach does not permit the prediction of the phase lag between the prescribed flapping motions and the wing's response in terms of bending deformation; which would improve the prediction capabilities of the computational tool significantly. In a recent work by the author's [15] the fully coupled 2-D BEM-FEM scheme is proposed for the hydroelastic analysis of flapping-foil thrusters and it is found to be in excellent agreement with experimental data found in the literature. Finally, the tools developed for the present work serve as the building blocks for the fully coupled 3-D BEM-FEM scheme for hydroelastic analysis and optimization that is currently under study.

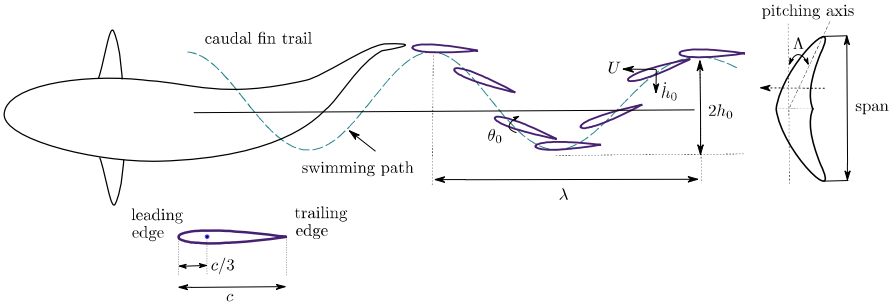

Figure 1. Schematic representation of the flapping wing kinematics (heaving, pitching motions) inspired by the *thunniform* swimming mode, adapted from [1].

2. Flapping wing kinematics

In this work we consider a 3-D wing operating in thrust-producing mode that undergoes prescribed motions, i.e. a forward motion at constant speed U , a harmonic heaving motion and a harmonic pitching

motion with respect to a pivot point placed at $c/3$ from the leading edge; as shown in Figure 1. The heave and pitch motions are respectively,

$$h(t) = h_o \sin(\omega t),\ \theta(t) = \theta_o \sin(\omega t + \psi) \tag{1}$$

whereas the forward motion in the direction of the negative *x*-axis is defined as

$$s(t) = -Ut \tag{2}$$

with h_o, θ_o denoting the heave, pitch amplitudes, ω the frequency and ψ the phase lag; a key parameter for operation in a thrust-producing mode. Based on the literature, we have selected $\psi = -90\,\text{deg}$; see [2]. We introduce a body-fixed coordinate system denoted as *xyz* and a global coordinate system *XYZ*. The y-axis and x-axis of the body-fixed coordinate system are defined as the spanwise and the chordwise directions of the wing respectively. The axis centre is placed at the leading edge in the root section. The wing is made of a homogeneous and isotropic material and is free to deform under hydrodynamic and inertial forces. At each time instance the deformed geometry $\{x^i\}$ in the body-fixed coordinate system *xyz* can be mapped to the global coordinate system via the following transformation,

$$\{X^i\} = f_s(t)\left([Q^i]\cdot\{x^i\} + \{\Delta^i\}\right), \tag{3}$$

$$[Q^i] = \begin{bmatrix} \cos\theta(t) & 0 & -\sin\theta(t) \\ 0 & 1 & 0 \\ \sin\theta(t) & 0 & \cos\theta(t) \end{bmatrix}, \{\Delta^i\} = \begin{bmatrix} s(t) \\ 0 \\ h(t) \end{bmatrix}, \tag{4}$$

where $f_s(t) = 1 - \exp(-f_o(t/T)^2), f_o = 1.5$ is a filter function permitting smooth transition between rest and a fully developed state of oscillatory motions. In the body-fixed coordinate system $\{x_o\}$ refers to the reference undeformed geometry and $\{x^i\}$ to the deformed state. The wing in the global coordinate system is denoted by $\{X^i\}$ as shown in figure 2.

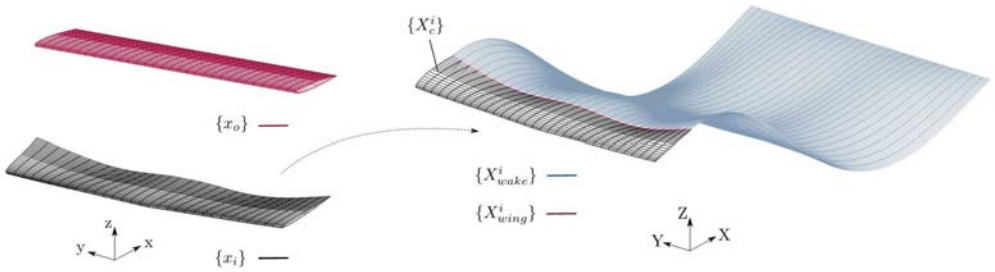

Figure 2. Schematic representation of the flapping wing thruster in the body-fixed coordinate system xyz (mechanics) and the global coordinate system XYZ (hydrodynamics).

3. Materials and Methods

Depending on the geometry of the examined flapping wing, certain assumptions can be made regarding the structural idealization. In the present, we assume that the thickness of the hydrofoil sections is sufficiently small compared to the main dimensions (chord, span), therefore a Kirchhoff thin plate model is selected. This model is suitable for the prediction of the wing's response in terms of bending and since it has been reported in the literature that chordwise and spanwise bending can contribute to the efficiency enhancement of wings operating as thrusters; see also [16], [8] and [9], this idealization can be justified. For the prediction of hydrodynamic loads that act on the structure due to the enforced flapping motion of the wing, we implement an unsteady lifting flow model for 3-D incompressible, inviscid and

irrotational fluid flows [17]. The rotational part of the flow is restricted in the trailing-vortex sheet emanating from the sharp trailing edge. The flapping wing is fully submerged within the fluid medium, the free-stream velocity is taken as zero and interactions with the free surface or other bodies/boundaries are neglected. In the sections that follow, we present briefly the structural dynamics of the flapping wing, the mathematical formulation behind the selected hydrodynamic model, details regarding the propulsive performance metrics and finally the coupling scheme.

3.1. Structural dynamics

The passive deformation caused by hydrodynamic pressure and inertial forces is solved in the local coordinate system xyz using the Kirchhoff's plate model known as Classical Plate Theory (CPT), based on the small displacements assumption. A direct consequence of the employed strain-displacement relation of CPT is the zeroing of shear deformation that restricts the applicability of the theory in 'thin' configurations; see [18] for higher-order plate theories allow varying degrees of shear deformation. The vertical bending equation of motion (in the z-direction) for plates with variable flexural rigidity is the following 4rth order PDE,

$$D\nabla^4 w+\nabla^2 D\cdot\nabla^2 w+2\nabla D\cdot\nabla\left(\nabla^2 w\right) \tag{5}$$
$$-(1-v)\left(\partial_x^2 D\partial_y^2 w-2\partial_x\partial_y D\partial_x\partial_y w+\partial_y^2 D\partial_x^2 w\right)+\rho_s\tau(x)\partial_t^2 w=q_h\left(x;t\right)+q_f\left(x;t\right)$$

with chordwise hydrodynamic pressure difference term and fictitious forces due to the non-inertial motions enforced to the pivot point given respectively by

$$q_h(x;t)=0.5\rho_f U^2\Delta C_p,\ \ q_f(x;t)=-\rho_s\tau(x)\left(x\cdot\ddot{\theta}(t)+\ddot{h}(t)\cos\theta(t)\right) \tag{6}$$

where $D(x,y)=\dfrac{E\tau^3(x)/}{12(1-v^2)}$ denotes the flexural rigidity, E Young's modulus, v Poisson ratio, ρ_s the material density, $\tau(x)$ the plate thickness distribution and $\theta(t),h(t)$ the pitch/heave motion amplitudes. Details regarding the derivation of the resulting fictitious forces can be found in [15]. The above *fourth order* PDE is complimented by a set of natural and/or essential conditions on each edge; see Table 1. Essential conditions involve the primary variables, which in this case are the deflection w (vertical motion) and the rotations $\partial_x w,\partial_y w$ and express geometric considerations. Natural conditions involve expressions of secondary variables which are known as stress resultants and stress couples referring to shear forces, bending and twisting moments.

The numerical treatment of equation (5) is sought after by means of FEM that essentially targets the equivalent C^1 variational problem. The smoothness requirements on the approximate solution poses a problem as the construction of conforming FEM schemes becomes challenging. Interesting accounts on the subject can be found in [19]. For the numerical solution we have developed a finite element solver (FEM) based on DKT (Discrete Kirchhoff Triangle) elements. The DKT follows a C^0 formulation (Reissner-Mindlin) and satisfies the geometric Kirchhoff assumptions. The extended global equation that is derived from the Galerkin scheme using FEM assembly techniques, local-to-global numbering and Gaussian quadrature is

$$\mathbf{M}_{glob}\ddot{\mathbf{U}}+\mathbf{C}\dot{\mathbf{U}}+\mathbf{K}_{glob}\mathbf{U}=\mathbf{F} \tag{7}$$

where $\mathbf{M}_{glob}$, $\mathbf{K}_{glob}$ stand for the global mass and stiffness matrices respectively, $\mathbf{F}_{glob}$ is the global load vector and $\mathbf{U}=[w^i,b^i{}_x,b^i{}_y,\ldots]'$ is the vector containing the nodal unknowns for the partitioned domain Ω^h. The selected boundary conditions are formulated by means of Lagrange multipliers and lead to an extension of the system of discretized equations; [20]. For the Delauney triangulation we used the

Matlab 2022a PDE Toolbox [21]. Regarding the proportional damping $\mathbf{C} = \alpha_1 \mathbf{M}_{glob} + \alpha_2 \mathbf{K}_{glob}$ the coefficients are defined using available experimental data. For the time-integration of the above 2nd order PDE in equation (7) we use the Newmark Method with $\gamma = 0.5,\ \beta = 0.25$, where

$$\begin{aligned} \dot{\mathbf{U}}_{n+1} &= \dot{\mathbf{U}}_n + (1-\gamma) dt \ddot{\mathbf{U}}_n + \gamma dt \ddot{\mathbf{U}}_{n+1} \\ \mathbf{U}_{n+1} &= \mathbf{U}_n + dt \dot{\mathbf{U}}_n + dt^2 \left(\frac{1}{2} - \beta \right) \ddot{\mathbf{U}}_n + dt^2 \ddot{\mathbf{U}}_{n+1} \end{aligned} \tag{8}$$

Table 1. Common edge boundary conditions.

Clamped (C)	$w = 0,\ \partial_n w = 0$
Simply supported (S)	$w = 0,\ \ M_{nn} = 0$
Free (F)	$V_n = Q_n + \partial_s M_{ns} = 0,\ M_{nn} = 0$

3.2. Hydrodynamic model

The wing and wake boundaries, denoted by $\partial D_B(t)$ and $\partial D_W(t)$ respectively, are modelled as surfaces of potential discontinuity in the global coordinate system XYZ. The wing surface undergoes prescribed rigid-body motions and is free to deform passively. The wake boundary represents the trailing vortex sheet that emanates from the sharp trailing edge which is modelled as a free shear layer with non-zero vorticity. The formulation of the initial boundary value problem (IBVP) problem is based on potential theory and boundary integral equations (BIE). The governing equation for the total velocity potential is the Laplace equation

$$\Delta \Phi(\mathbf{x};t) = 0,\ \mathbf{x} \in D(t) \tag{9}$$

For this boundary value problem, a flow-tangency condition must hold on the wing boundary

$$\partial_n \Phi(\mathbf{x};t) = \mathbf{V}_B(\mathbf{x};t) \cdot \mathbf{n}(\mathbf{x};t),\ \mathbf{x} \in \partial D_B(\mathrm{t}) \tag{10}$$

where $\partial_n \Phi(\mathbf{x};t) = \nabla \Phi(\mathbf{x};t) \cdot \mathbf{n}$ denotes the normal derivative with $\mathbf{n}$ the unit normal vector on the body and $\mathbf{V}_B(\mathbf{x};t)$ the instantaneous velocity of the wing due to oscillatory motions and elastic displacement. To close the problem a non-linear (quadratic), pressure-type Kutta condition, requiring zero pressure difference at the trailing edge is enforced,

$$\partial_t (\Phi^u - \Phi^l) + 0.5(\nabla \Phi^u + \nabla \Phi^l) \cdot (\nabla \Phi^u - \nabla \Phi^l) = 0, \tag{11}$$

The above form of the pressure-type Kutta condition can be derived by using the approximate Bernoulli's theorem on the body at upper and lower sides of trailing edge along with the assumption that the trailing wake evolves in time as a material curve (based on the mean velocity). The approximate Bernoulli's theorem is,

$$\frac{p(\mathbf{x};t)}{\rho_f} + \partial_t \Phi(\mathbf{x};t) + \frac{1}{2} \left[\nabla \Phi(\mathbf{x};t) \right]^2 = 0,\ \ \mathbf{x} \in \partial D \tag{12}$$

More details can be found in [17]. A linearization of the above yields a simplified wake model, where the generated vortex sheet emanates parallel to the bisector of the trailing edge and has the shape of trailing edge's path. The weakly singular Boundary Integral Equation (BIE), which holds for each $\mathbf{x}_o \in \partial D_B(t)$, is derived for the present formulation,

$$\frac{1}{2} \Phi_B(\mathbf{x}_0;t) + \int_{\partial D_B(t)} \Phi_B(\mathbf{x}_0;t) \partial_n G(\mathbf{x}_0 \mid \mathbf{x}) \mathrm{ds}(\mathbf{x}) = \int_{\partial D_B(t)} b(\mathbf{x}_0;t) G(\mathbf{x}_0 \mid \mathbf{x}) \mathrm{ds}(\mathbf{x}) - \int_{\partial D_W(t)} \mu_W(\mathbf{x}_0;t) \partial_n G(\mathbf{x}_0 \mid \mathbf{x}) \mathrm{ds}(\mathbf{x}) \tag{13}$$

with μ_W denoting the dipole intensity on the wake (or equivalently the potential jump) and $G(\mathbf{x}_0 \mid \mathbf{x})$ the Green function for the 3-D Laplace equation.

For the numerical solution of the 3-D unsteady and nonlinear problem an efficient (in terms of both time and space complexity) GPU-accelerated boundary element method (BEM) is developed, based on a formulation that is direct with respect to the potential. Particularly, the pressure-type Kutta condition is the basis for the construction of the dynamical system equation and the other kinematic boundary conditions provide appropriate constraints. Particularly, the discretized version of equation (13) based on a low-order piecewise-constant approximation, is used as an algebraic constraint by means of the DtN (Dirichlet-to-Neumann) operator. Starting from a prescribed initial condition, e.g. from rest, a time-stepping method is applied to obtain the numerical solution. Particularly, the higher-order Adams-Bashforth-Moulton predictor-corrector method provides the required accuracy, stability and efficiency. The calculation of generalised forces is obtained without any further assumption by pressure integration. The latter is calculated by using an approximate Bernoulli equation; see [17] for more details.

3.2.1. Propulsive performance metrics

The instantaneous lift, thrust and moment (with respect to the selected pivot axis) can be calculated using the following formulas,

$$C_L = \frac{L(t)}{0.5\rho U^2 cs} = -\frac{1}{A}\int_{\partial D_B} C_p \mathbf{n}\cdot\hat{\mathbf{y}}ds, \quad C_T = \frac{T(t)}{0.5\rho U^2 cs} = \frac{1}{A}\int_{\partial D_B} C_p \mathbf{n}\cdot\hat{\mathbf{x}}ds, \quad C_M = \frac{M(t)}{0.5\rho U^2 c^2 s} = -\frac{1}{Ac}\int_{\partial D_B} C_p \mathbf{n}\cdot\mathbf{r}(s;t)ds, \tag{14}$$

where A denotes the planform area and $\mathbf{r}(s;t)$ the reference vector for the moment coefficient calculation. The propulsive efficiency (or Froude efficiency) metric is calculated as the ratio between the power output and input,

$$\eta = \frac{\bar{C}_{Pout}}{\bar{C}_{Pin}}, \ \bar{C}_{Pout} = \frac{P_{out}}{0.5\rho U^3 A}, \ \bar{C}_{Pin} = \frac{P_{in}}{0.5\rho U^3 A} \tag{15}$$

$$P_{out} = \frac{1}{T_p U}\int_0^{T_p} T(t)Udt, \quad P_{in} = \frac{1}{T_p U}\int_0^{T_p} L(t)\dot{h}(t) + M(t)\dot{\theta}(t)dt \tag{16}$$

where T_p is harmonic motion period, T(t) the instantaneous thrust and U the forward motion velocity; see also [2]. The power input metric is an estimate for the required power to sustain the enforced flapping-foil kinematics; see also [2].

3.3. Fluid-structure interaction

In this work, we propose a partitioned BEM-FEM numerical scheme for the prediction of the hydroelastic analysis of flexible flapping-foil thrusters. The term partitioned refers to the use of two distinct computational tools that can be used independently and for the treatment of the fluid-structure interaction (FSI) problem are coupled via data exchange and internal iteration loops. The weak coupling scheme we implement consists of the following steps:

1. First, we performed a three flapping-cycle simulation using the GPU-BEM solver for the un-deformed wing to extract the time history of the hydrodynamic pressure difference.
2. The hydrodynamic pressure data are mapped via interpolation to the FEM unstructured mesh.
3. Then, we simulate the structural response of the wing with FEM using the hydrodynamic pressure data to obtain predictions for the deformation amplitude.
4. Finally, we performed a GPU-BEM simulation using the deformed geometry as obtained from the FEM solution to obtain an estimate for the hydrodynamic forces and via integration for the propulsive performance metrics.

This weak coupling approach can produce valuable estimates for the elastic wing's response under hydrodynamic loads, but it is not recommended for phase lag predictions between the flapping motions and the wing's response, especially for highly unsteady flows. The prediction capabilities and the limitations of the weakly coupled BEM-FEM are discussed. Finally, the proposed GPU-BEM and FEM numerical tools serve as the building blocks for the fully coupled 3-D BEM-FEM scheme for the hydro-elastic analysis and optimization of flapping-foil thrusters that is currently under development; see, e.g. a previous work by the author's for the 2-D case [15]. Additional information about the coupling approach can be found in [22].

4. Numerical results

All computations were performed on an AMD Ryzen 9 3900XT workstation equipped with an NVDIA GeForce RTX 3080 graphics card. Leading edge separation and tip vortex rollup modelling is not included in the present BEM formulation. The propulsive performance metrics correspond to the average values during the last flapping cycle of a three-period simulation. For the verification of the developed GPU-BEM solver that is suitable for the prediction of the hydrodynamic pressure and integrated loads for wing that undergo arbitrary but known morphing (i.e. active deformation) can be found in [23]. Detailed results concerning the validation of the FEM solver are omitted for brevity, however some indicative comparisons can be found in [20]. Regarding the discretization, we used NEC= 50 (chordwise), NEA = 5AR (spanwise) panel elements for the GPU-BEM spatial discretization, N_{FEM}=1800 DKT triangles for the FEM mesh and a time discretization of dt = $0.50T_p$ for both solvers.

4.1. Passively deforming heaving wing

In [16], the response of rectangular wings with main dimensions c=100mm (chord), s=600mm (span) and NACA0012 hydrofoil sections in pure heaving is investigated experimentally. The root displacement is given by $h(t) = \alpha_{root} \cos(\omega t)$. The wings tested were constructed using different materials, which led to observations of passive bending deformation. As reported, the dominant bending mode was of first order and in the publication the tip bending amplitude and phase are provided. This is quite useful for comparisons with active bending deformation; see, e.g. [23]. The inflexible wing was manufactured in a way that restricts deformations in all directions, however some deformations were observed. Regarding the numerical computations, the inflexible wing is treated as rigid, whereas the flexible wing is modelled as a steel sheet with 1mm thickness. Both wings are clamped at the root section. We simulate the whole wing the GPU-BEM solver with dimensions c=100mm and s=600mm, however for the structural response we simulate with the FEM solver the half wing with boundary conditions (FFFC). The heaving amplitude is $\alpha_{root} = 0.175c$, $\mathrm{Re} = Uc/\nu = 30,000$ with viscosity $\nu = 10^{-6} m^2/s$ and the constant inflow velocity $U = 0.3m/s$. The forcing frequency is defined as $k_G = \pi fc/U$ where $\omega = 2\pi f$.

In figure 3, we compare the weakly coupled BEM-FEM scheme with the experimental results for the case of an inflexible and a flexible wing. We can observe that the weakly coupled BEM-FEM scheme is capable of reproducing trends regarding the effects of forcing frequency and material properties on the average thrust coefficient. The differences between our predictions for the inflexible wing are attributed to the fact that in the experiments the inflexible wing undergoes bending deformation (with reported tip phase and amplitude) that provides additional thrust. It is typical for potential solvers to overestimate the thrust if viscous corrections are not included in the modelling (i.e. the present GPU-BEM), however it is evident from the differences between our predictions; which underestimate the thrust generated from the flexible wing, that accurate predictions of the phase lag between the heaving motion and the deformation are essential for better estimates. The weakly coupled BEM-FEM however, is capable of reproducing trends for the propulsive efficiency. In figure 3, there is a region of small forcing frequencies indicating that the flexible wing is slightly more efficient than the inflexible (rigid) wing, however for larger values of the forcing frequency the opposite happens. In figure 4, we compare the time history of the tip deformation for the inflexible (rigid) and the flexible wing. The amplitude

predictions are in good agreement; however, the phase lag is not predicted accurately. A strong coupling approach as in [15], can predict with acceptable accuracy the phase lag and thus produces better predictions overall. Finally, the deformation of the wing is provided for the eight instances (denoted with circles in figure 4) in figure 5 that follows.

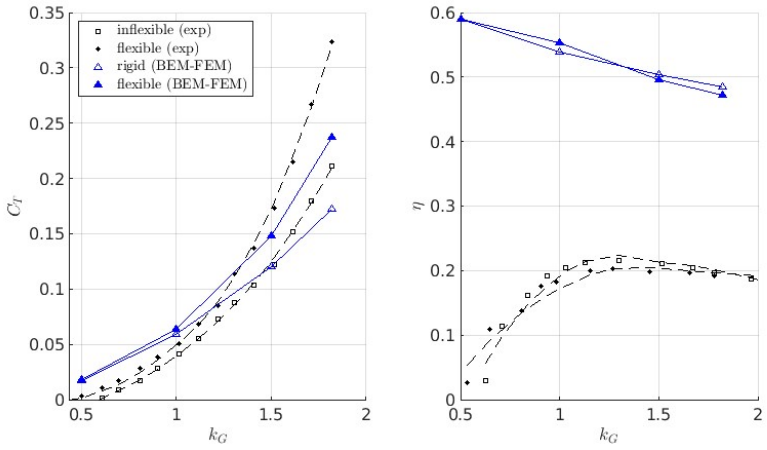

Figure 3. Thrust coefficient [left] and propulsive efficiency [right] as a function of frequency and comparison with the experimental results from [16]. Proportional damping coefficients $a = 0.17,\ b = 2.4510^{-4}$. Results for $k_G = \{0.5,\ 1.0,\ 1.5,\ 1.82\}$.

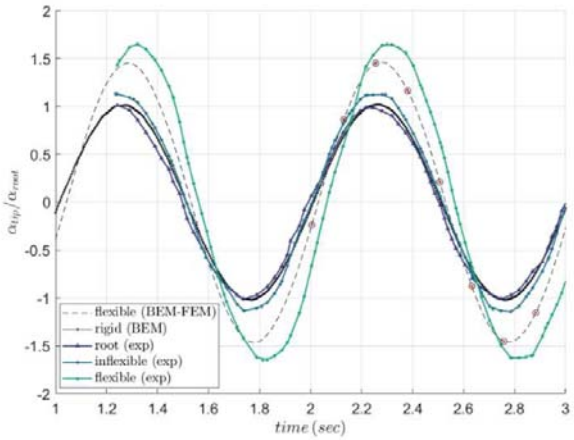

Figure 4. Time history of tip-displacements for the last two flapping-cycles for $k_G = 1.82$ .The red circles indicate time instances where the deformation of the half wing is provided in figure 5.

5. Conclusion

In this work we investigate the capabilities and the limitations of a weakly coupled BEM-FEM scheme for the hydroelastic analysis of flapping-foil thrusters via comparison with experimental data from [16]. The BEM solver is based on a 3-D unsteady lifting flow formulation suitable for the prediction of the hydrodynamic pressure of morphing wings. Regarding the structural dynamics, the wing is idealized as a thin plate and numerical predictions are obtained via FEM formulation based on Discrete Kirchhoff triangles (DKT). The developed computational tool is suitable for predictions of amplitude predictions and trends regarding the thrust coefficient and propulsive efficiency for the case of passively deforming flapping wings in pure heaving. However, it not suggested for phase lag estimation between the enforced

kinematics and the elastic deformations. Finally, the extension of the present partitioned 3-D BEM-FEM scheme using full coupling is proposed for future work and currently under study.

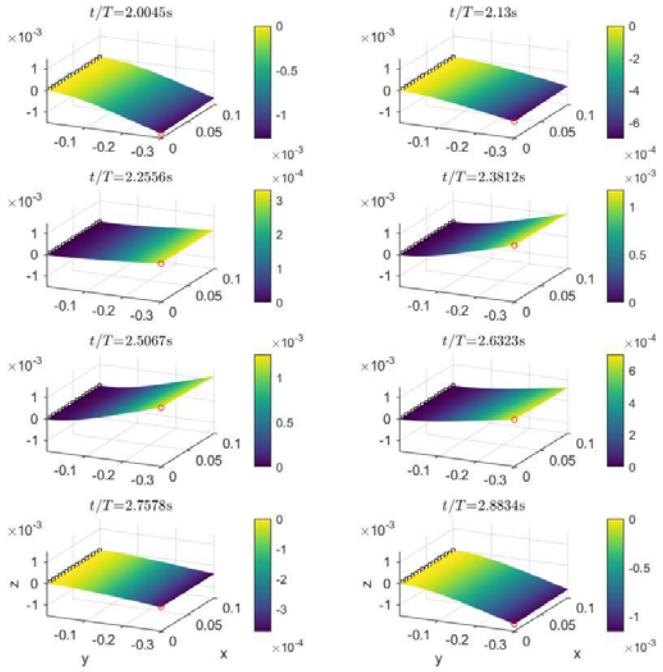

Figure 5. The deformation of a half wing as obtained with the weakly coupled BEM-FEM for $k_G = 1.82$. The wing is clamped at the root section as shown with black squares in the subfigures.

Acknowledgments
The present work is supported by the SeaTech H2020 project and has received funding from the European Union's Horizon 2020 research and innovation program under the grant agreement No 857840. The opinions expressed in this document reflect only the author's view and in no way reflect the European Commission's opinions. The European Commission is not responsible for any use that may be made of the information it contains. Ms. D. Anevlavi is a recipient of the Special Account for Research Funding (E.L.K.E.) of National Technical University of Athens (N.T.U.A.) Scholarship Program for doctoral studies.

References

[1] Sfakiotakis M, Lane D and Davies J 1999 Review of fish swimming modes for aquatic locomotion *IEEE Journal of Oceanic Engineering* **24**(2) 237–252.

[2] Triantafyllou M S, Hover F, Techet A and Yue D 2005 Review of hydrodynamic scaling laws in aquatic locomotion and fishlike swimming *ASME. Appl. Mech. Rev.* **58** 226–237.

[3] Yu D, Sun X, Bian X, Huang D and Zheng Z 2017 Numerical study of the effect of motion parameters on propulsive efficiency for an oscillating airfoil *Journal of Fluids and Structures* **68** 245-263.

[4] Barrett D S 1996 Propulsive efficiency of a flexible hull underwater vehicle *Ph.D. Thesis, Massachusetts: Department of Ocean Engineering MIT*.

[5] Ntouras D, Papadakis G and Belibassakis K 2022 Ship bow wings with application to trim and resistance control in calm water and in waves *Journal of Science and Marine Engineering,* **10**(4) 492.

[6] Belibassakis K, Filippas E and Papadakis G 2021 Numerical and experimental investigation of the performance of dynamic wing for augmenting ship propulsion in head and quartering seas *Journal of Marine Science and Engineering,* **10**(1) 24.

[7] Shyy W, Aono H, Chimakurthi S, Trizila P, Kang C K, Cesnik C and Liu H 2014 Recent progress in flapping wing aerodynamics and aeroelasticity *Engineering Analysis with Boundary Elements* **46**(7) 284–327.

[8] Quinn D B, Lauder G V and Smits A J 2015 Maximizing the efficiency of a flexible propulsor using experimental optimization *J. Fluid Mech.* **767** 430-448.

[9] Richards A J and Oshkai P 2015 Effect of stiffness, inertia and oscillation kinematics on the thrust generation and efficiency of an oscillating-foil propulsion system *J. Fluids and Structures* **57** 357-374.

[10] Korobkin A, Parau E I and Vanden-Broek J M 2011 The mathematical challenges and modelling of hydroelasticity *Phil. Trans. R. Soc. A.* **369**(1947) 2803-2812.

[11] Heo H, Ju J and Kim D M 2013 Compliant cellular structures: Application to a passive morphing airfoil *Composite Structures* **106** 560-569.

[12] Manudha B G P, Herath T, Phillips A W and John N S 2017 Structural strength and laminate optimization of self-twisting composite hydrofoils using a Genetic Algorithm *Composite Structures* **176** 359-378.

[13] Zhu Q 2007 Numerical simulation of a flapping foil with chordwise or spanwise flexibility *AIAA Journal* **45**(10) 2448-2457.

[14] Vanilla T T, Benoit A and Benoit P 2021 Hydro-elastic response of composite hydrofoil with FSI *Ocean Engineering* **221** 108230.

[15] Anevlavi D E, Filippas E S, Karperaki A E and Belibassakis K A 2020 A non-linear BEM–FEM coupled scheme for the performance of flexible flapping-foil thrusters *Journal of Marine Science and Engineering* **8**(1) 56.

[16] Heathcote S, Wang Z and Gursul I 2008 Effect of spanwise flexibility on flapping wing propulsion *Journal of Fluids and Structures* **24**(2) 183-199.

[17] Filippas E 2019 Hydrodynamic analysis of ship and marine biomimetic systems in waves using GPGPU programming *Ph.D. Thesis School of Naval Architecture and Marine Engineering, NTUA*.

[18] Reddy J 2006 Theory and analysis of elastic plates and shells *Boca Raton: CRC Press*.

[19] Zienkiewicz O, Taylor R, Papadopoulos P and Oñate E 1990 Plate bending elements with discrete constraints: New triangular elements *Computers & Structures* **35**(4) 505-522.

[20] Karperaki A 2021 Hydroelastic interaction between ocean waves and large floating structures in the inhomogeneous ocean environment *Ph.D. Thesis, School of Naval Architecture and Marine Engineering, NTUA*.

[21] MATLAB Ver. 2022a Software Package *The Mathworks, Inc. Natick MA*.

[22] Priovolos A, Filippas E and Belibassakis K 2018 A vortex-based method for improved flexible flapping-foil thruster performance *Engineering Analysis with Boundary Elements* **95** 69-84.

[23] Anevlavi D, Filippas E and Belibassakis K 2023 Energy-minimizing kinematics for actively morphing flapping-foil thrusters *The 8th International Symposium on Ship Operations, Management & Economics (SOME) Athens, Greece*.